

# Adaptive Label Correction for Robust Medical Image Segmentation with Noisy Labels

Chengxuan Qian<sup>1</sup>, Kai Han<sup>1</sup>, Siqi Ma<sup>1</sup>, Chongwen Lyu<sup>1</sup>, Zhenlong Yuan<sup>2</sup>, Jun Chen<sup>1</sup>, Zhe Liu<sup>1,†</sup>

<sup>1</sup>School of Computer Science and Communication engineering, Jiangsu University    <sup>2</sup>Lenovo Research  
chengxuan.qian@stmail.ujs.edu.cn, zliu@ujs.edu.cn

**Abstract**—Deep learning has shown remarkable success in medical image analysis, but its reliance on large volumes of high-quality labeled data limits its applicability. While noisy labeled data are easier to obtain, directly incorporating them into training can degrade model performance. To address this challenge, we propose a Mean Teacher-based Adaptive Label Correction (ALC) self-ensemble framework for robust medical image segmentation with noisy labels. The framework leverages the Mean Teacher architecture to ensure consistent learning under noise perturbations. It includes an adaptive label refinement mechanism that dynamically captures and weights differences across multiple disturbance versions to enhance the quality of noisy labels. Additionally, a sample-level uncertainty-based label selection algorithm is introduced to prioritize high-confidence samples for network updates, mitigating the impact of noisy annotations. Consistency learning is integrated to align the predictions of the student and teacher networks, further enhancing model robustness. Extensive experiments on two public datasets demonstrate the effectiveness of the proposed framework, showing significant improvements in segmentation performance. By fully exploiting the strengths of the Mean Teacher structure, the ALC framework effectively processes noisy labels, adapts to challenging scenarios, and achieves competitive results compared to state-of-the-art methods.

## I. INTRODUCTION

Medical image segmentation is essential for disease diagnosis and treatment planning. While deep learning has significantly advanced this field, its success relies heavily on large volumes of high-quality annotated data [1], [2], [3]. However, manual annotation is not only time-consuming but also susceptible to noise due to the complexity of medical images and variations in expertise [4]. Although crowd-sourcing or machine-generated labels can reduce costs, their low quality often misguides models, undermining the advantages of high-quality annotations and degrading overall performance. Effectively utilizing noisy labeled data thus remains a critical challenge for advancing medical image segmentation.

In recent years, methods on learning with noisy labels have primarily focused on two paradigms: label quality-agnostic and label quality-aware approaches. In label quality-agnostic methods, all labels, regardless of their source or quality, are treated equally. For instance, [5], [6] assume that labels of varying quality originate from different sources and therefore mix all label data during training. Specifically, [5] integrated confident learning into a teacher-student framework to identify corrupted labels, equipping the model with resilience against noise. Similarly, [6] proposed addressing annotation noise in medical image segmentation by leveraging reliable mutual

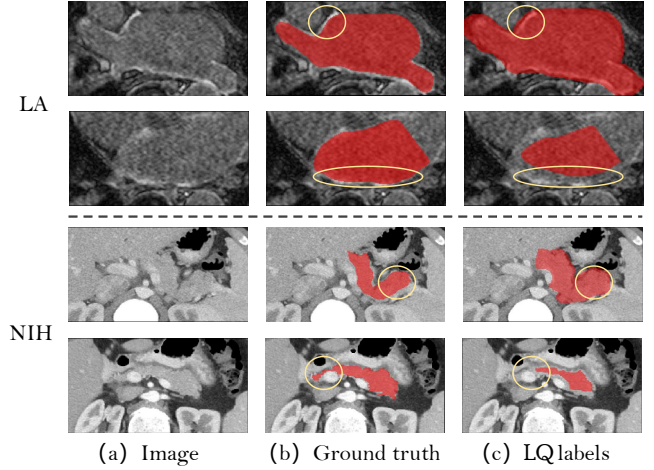


Fig. 1. Visualization of noisy labels: The first and third rows display LQ labels from ground truth expansion, while the second and fourth rows depict those from ground truth erosion.

distillation between dual segmentation models. Additionally, [7] introduced a two-stage weakly supervised approach for 3D medical image segmentation using only seven annotated points per volume. This method employs a self-and-cross-monitoring strategy, combining self-training with cross-knowledge distillation to mitigate noise in pseudo labels. In contrast, label quality-aware methods differentiate between labels of varying quality and leverage this distinction to enhance network training [8], [9], [10]. For example, [11] formalized the distinction between the two paradigms, demonstrating that label quality-aware methods generally outperform their agnostic counterparts. These methods often rely on uncertainty estimation techniques, such as data or network dropout, to assess label quality. However, these approaches fail to fully capture the subtle differences between various disturbance versions and lack the adaptability of a self-ensemble architecture to dynamically correct low-quality labels.

In this paper, we propose an Adaptive Label Correction (ALC) self-ensemble architecture for robust medical image segmentation with noisy labels, leveraging the Mean Teacher structure to effectively address the challenges of noisy labels. Unlike traditional methods that rely primarily on uncertainty to evaluate label quality, our approach incorporates an adaptive label correction mechanism that dynamically captures and weights differences between various perturbation versions, improving label reliability. To further strengthen the trustworthiness of the training process, we introduce a sample-level

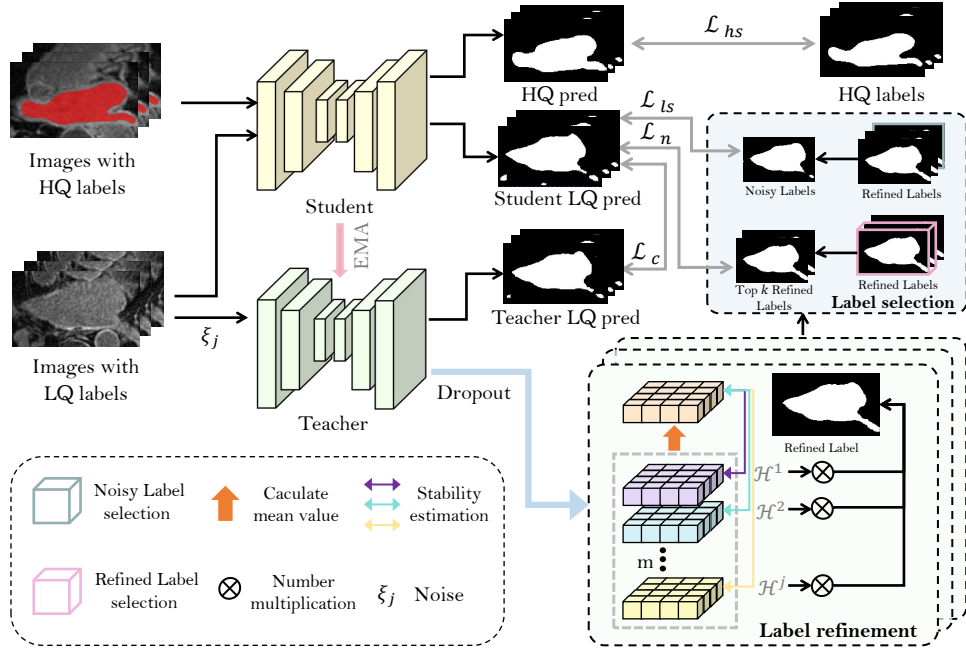


Fig. 2. Overview of our proposed ALC approach, which employs a student-teacher network to integrate label correction and selection. The total loss comprising high-quality label loss  $\mathcal{L}_{hs}$ , low-quality label loss  $\mathcal{L}_{ls}$ , noisy label loss  $\mathcal{L}_n$ , and consistency loss  $\mathcal{L}_c$ .

uncertainty-based label selection strategy, prioritizing high-confidence samples for gradient updates. The Mean Teacher framework, with its consistency learning and lightweight design through exponential moving average (EMA), enables the efficient extraction of latent semantic information from low-quality labels, facilitates dynamic noise correction, and ensures computational efficiency. Extensive experiments validate that our method surpasses state-of-the-art approaches in handling noisy label scenarios, providing enhanced robustness and adaptability for medical image segmentation.

## II. METHODOLOGY

The proposed Adaptive Label Correction (ALC) framework effectively mitigates the impact of noisy labels by leveraging HQ labels for reliable supervision and refining LQ labels to uncover latent semantic information. The framework achieves this through three core components: 1) **HQ Label Learning**, which provides a solid foundation for accurate segmentation using clean annotations; 2) **LQ Label Learning**, which refines noisy labels through adaptive weighting and selects high-confidence samples via uncertainty-based evaluation to reduce noise interference; and 3) **Consistency Learning**, which utilizes a student-teacher network to align predictions under perturbations, enhancing model robustness. By dynamically integrating these components, the framework extracts optimal supervision and semantic insights, delivering superior performance in medical image segmentation.

### A. Learning from high-quality labeled data

Given a dataset  $D$  comprising a high-quality (HQ) label dataset  $D_h = \{(X_h^i, Y_h^i)\}_{i=1}^{N_h}$  and a low-quality (LQ) label dataset  $D_n = \{(X_n^i, Y_n^i)\}_{i=1}^{N_n}$ , where  $X, Y$  represent images

and their corresponding labels, and  $N_h$  and  $N_n$  denote the numbers of HQ and LQ label samples, respectively. Our objective is to leverage HQ labels for reliable baseline predictions and refining LQ labels to extract latent semantic information, enhancing overall model learning.

To tackle the challenges of noisy and inconsistent annotations in medical image segmentation, the proposed framework leverages high-quality (HQ) labels to provide reliable supervision and establish a robust baseline. HQ labels ensure accurate and consistent training by guiding the student network to minimize the segmentation loss:

$$\mathcal{L}_{hs} = \frac{1}{B_h} \sum_{i=1}^{B_h} \ell_{seg}(f_{\theta_s}(X_h^i), Y_h^i) \quad (1)$$

where  $f_{\theta_s}$  represents the student network parameterized by  $\theta_s$ ,  $B_h$  is the batch size of HQ labeled data. The segmentation loss  $\ell_{seg}$  is formulated as a weighted combination of Cross Entropy loss  $\ell_{ce}$  and Dice loss  $\ell_{dice}$ :

$$\ell_{seg} = \frac{1}{2}(\ell_{ce} + \ell_{dice}) \quad (2)$$

The loss formulation combines  $\ell_{ce}$  for pixel-wise accuracy and  $\ell_{dice}$  for structural alignment, balancing fine-grained precision with segmentation robustness. This approach leverages HQ labels for consistent supervision, establishing a strong baseline to effectively integrate LQ labels and their latent semantic information.

### B. Learning from low-quality label data

The proposed framework addresses the challenges of low-quality (LQ) labels by introducing two key processes: Label Refinement and Label Selection. These processes aim to refine

noisy annotations and prioritize reliable samples, effectively mitigating the adverse effects of label noise while fully leveraging the latent semantic information in LQ data.

1) *Label Refinement*: Low-quality labels often suffer from noise and inconsistencies, requiring an effective refinement process to enhance their reliability. The framework employs multiple dropout operations [12] to simulate perturbations and extract stable features, leveraging the teacher network  $f_{\theta_t}$  to generate  $m$  probabilistic outputs  $\Psi$ :

$$\Psi^{i,j} = f_{\theta_t}(X_n^i + \xi_j), j \in \{1, \dots, m\} \quad (3)$$

where  $i$ ,  $j$ ,  $m$  and  $\xi$  represent the sample index, dropout index, number of dropout operations, and Gaussian noise, respectively. The voxel-level mean value  $\Psi_{avg}$  is then computed across all dropout outputs:

$$\Psi_{avg}^{i,(x,y,z)} = \frac{1}{m} \sum_{j=1}^m \Psi^{i,j,(x,y,z)} \quad (4)$$

where  $(x, y, z)$  denotes the spatial location index. To evaluate the stability of outputs at each voxel, Kullback–Leibler (KL) divergence is used:

$$\begin{aligned} \mathcal{H}^{j,(x,y,z)} &\approx KL(\Psi_{avg}^{i,(x,y,z)} \parallel \Psi^{i,j,(x,y,z)}) \\ &= \Psi_{avg}^{i,(x,y,z)} \log \frac{\Psi_{avg}^{i,(x,y,z)}}{\Psi^{i,j,(x,y,z)}} \end{aligned} \quad (5)$$

A higher  $\mathcal{H}^{j,(x,y,z)}$  value indicates greater uncertainty for the  $j$ -th output at voxel  $(x, y, z)$ . To adaptively refine labels, the outputs are fused using weights inversely proportional to their uncertainty:

$$\hat{Y}_{ref}^{i,(x,y,z)} = \arg \max_{k \in \{1, 2, \dots, C\}} \left[ \frac{1}{m} \sum_{j=1}^m \frac{\Psi^{i,j,(x,y,z)} e^{-\mathcal{H}^{j,(x,y,z)}}}{\sum_j e^{-\mathcal{H}^{j,(x,y,z)}}} \right] \quad (6)$$

where  $C$  is the number of segmentation classes. This refinement process improves label quality by dynamically weighting predictions based on their reliability.

2) *Label selection*: Despite label refinement, not all samples achieve sufficient quality for effective training. To further ensure reliability, a sample-level uncertainty-based selection algorithm is introduced. The uncertainty score  $\mathcal{U}^i$  for each sample is computed as:

$$\mathcal{U}^i = \frac{1}{N_{vox}} \sum_{x,y,z} \frac{1}{m} \left[ \sum_{j=1}^m \Psi^{i,j,(x,y,z)} - \left( \frac{1}{m} \sum_{j=1}^m \Psi^{i,j,(x,y,z)} \right) \right]^2 \quad (7)$$

Here,  $N_{vox} = W \cdot H \cdot Z$  represents the total number of voxel in the sample.  $W$ ,  $H$  and  $Z$  denote the spatial dimensions. Samples with the lowest uncertainty scores  $\mathcal{U}^i$  are prioritized for training. The top  $k$  samples are selected to compute the low-quality label loss  $\mathcal{L}_{ls}$ :

$$\mathcal{L}_{ls} = \frac{1}{k} \sum_{i=1}^k \ell_{seg}(f_{\theta_s}(X_n^i), \hat{Y}_{ref}) \quad (8)$$

where  $\ell_{seg}$  represents the segmentation loss.  $B_n$  is the batch size of noisy label data. Remaining samples, which may still contain noise, are used for noisy label loss  $\mathcal{L}_n$ :

$$\mathcal{L}_n = \frac{1}{B_n - k + 1} \sum_{i=k+1}^{B_n} \ell_{seg}(f_{\theta_s}(X_n^i), \hat{Y}_n) \quad (9)$$

### C. Consistency learning

To enhance model robustness and mitigate the effects of noise perturbations, the framework employs consistency learning through a student-teacher network architecture. This mechanism encourages alignment between the outputs of the student  $f_{\theta_s}$  and teacher  $f_{\theta_t}$  networks under different perturbation conditions. The consistency loss is defined as:

$$\mathcal{L}_c = \frac{1}{N_{vox}} \sum_{x,y,z} \left\| \sum_{j=1}^m f_{\theta_t}(X_n^{(x,y,z)}) - f_{\theta_s}(X_n^{(x,y,z)}) \right\| \quad (10)$$

It ensures that predictions from both networks remain stable and consistent across multiple dropout operations. Here,  $N_{vox}$  denotes the total number of voxels and  $m$  denotes the number of perturbation iterations.

---

**Algorithm 1** The training process of the overall framework.

---

**Input:** HQ label dataset  $(X_h, Y_h) \in D_h$ , LQ label dataset  $(X_n, Y_n) \in D_n$ ,  $k$ , model parameters  $\theta_t$  and  $\theta_s$ .

**Output:** model parameters  $\theta_s$  for inference.

```

1:  $t \leftarrow 0$ 
2: repeat
3:    $t \leftarrow t + 1$ ;
4:   for sample  $(X_i, Y_i)$  from  $D_h$  do  $\triangleright$  HQ label learning
5:     Compute  $\mathcal{L}_{hs}$  by Eq.(1);
6:   end for
7:   for sample  $(X^n, Y^n)$  from  $D_n$  do;  $\triangleright$  LQ label learning
8:     Evaluate voxel uncertainty by Eq. (3)-(5);
9:     Refine label by Eq. (6);
10:    Compute sample stability  $\mathcal{U}$  by Eq. (7);
11:    Select top  $k$  samples based on  $\mathcal{U}$ ;
12:    if sample  $i \in \text{top } k$  then
13:      Compute  $\mathcal{L}_{ls}$  by Eq. (8);
14:    else
15:      Compute  $\mathcal{L}_n$  by Eq. (9);
16:    end if
17:  end for
18:  Compute  $\mathcal{L}_c$  by Eq. (10);  $\triangleright$  Consistency learning
19:  Train with total loss  $\mathcal{L}_{total}$  by Eq. (11);
20: until the model converge.

```

---

### D. Total loss

The total loss integrates four key components to balance the contributions of different learning objectives: HQ label loss  $\mathcal{L}_{hs}$ , LQ label loss  $\mathcal{L}_{ls}$ , noisy label loss  $\mathcal{L}_n$ , and consistency loss  $\mathcal{L}_c$ . The total loss is expressed as:

$$\mathcal{L}_{total} = \mathcal{L}_{hs} + \lambda(t)(\alpha\mathcal{L}_{ls} + \beta\mathcal{L}_n + \mathcal{L}_c) \quad (11)$$

where  $\lambda(t)$  dynamically adjusts the weights during training, transitioning focus from HQ labels to LQ labels and consistency learning.  $\alpha$  and  $\beta$  controls the relative importance of  $\mathcal{L}_{ls}$  and  $\mathcal{L}_n$ , their sensitivity will be further analyzed in Section III-D and Fig. 6. This formulation ensures reliable supervision from HQ labels, effective utilization of LQ labels through refinement and robust learning, and stability via consistency constraints between student and teacher networks, enabling effective segmentation despite noisy annotations. The overall training process is shown in Algorithm 1.

### III. EXPERIMENTS

#### A. Datasets and Evaluation Metrics

**LA segmentation dataset.** The Left Atrium (LA) dataset [19] includes 100 GE-MRIs ( $0.625^3 \text{ mm}^3$  resolution). Following [20], 80 scans are for training and 20 for testing. Patches are  $112 \times 112 \times 80$ , with sliding window prediction for testing.

**NIH dataset.** The NIH pancreas dataset [21] has 82 CT scans. We use 62 for training and 20 for testing. Intensities are rescaled to  $[0, 1]$  within  $[-125, 275]$  HU, with  $96^3$  patches.

**Noisy label generation.** To simulate human errors, noisy labels are generated by randomly expanding or eroding ground truth by 3-15 pixels [11], [22], as shown in Fig. 1.

**Evaluation Metrics.** Following [11], [22], four metrics were employed to quantitatively evaluate segmentation performance: Dice Similarity Coefficient (Dice), Jaccard Index (Jaccard), 95% Hausdorff Distance (95HD), and Average Surface Distance (ASD). Upward ( $\uparrow$ ) and downward ( $\downarrow$ ) arrows indicate positive or negative indicators.

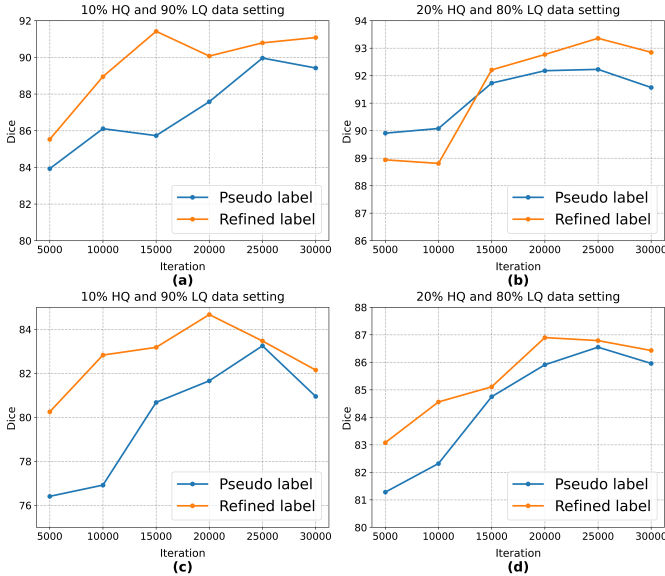


Fig. 3. Quantitative comparisons of pseudo and corrected label quality across iterations under varying HQ and LQ label ratios on the LA dataset (a)-(b) and NIH dataset (c)-(d).

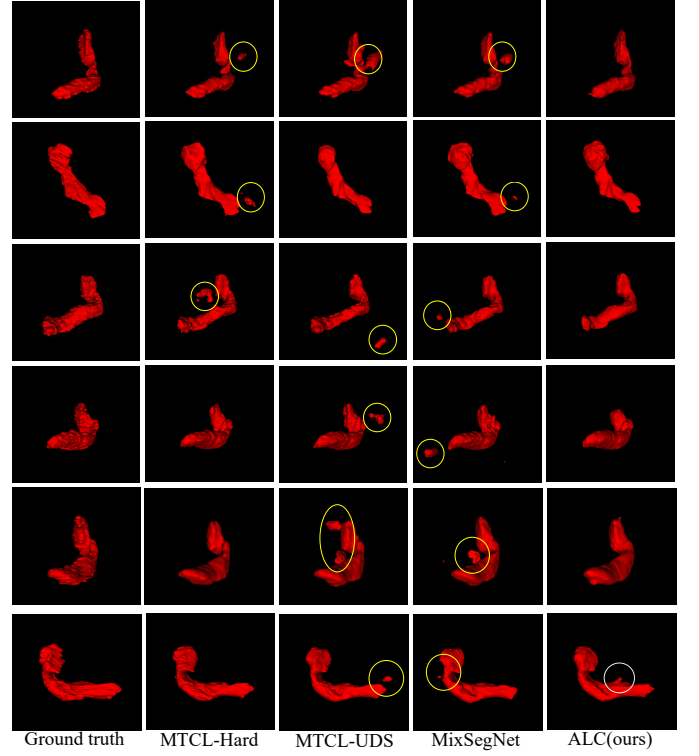


Fig. 4. Visual comparison of segmentation results on the NIH dataset under the 10% HQ and 90% LQ label setting across different methods

#### B. Implementation Details

The framework was implemented in PyTorch and run on an NVIDIA A6000 GPU with 48 GB memory. V-Net [23] served as the backbone within the Mean Teacher framework [24], with an EMA decay  $\gamma$  of 0.99. Network parameters were optimized using SGD. The batch size was set to 24, comprising 4 HQ label samples and 20 LQ label samples. Analysis of the  $k$  hyperparameter is presented in Section III-E. The code will be publicly released upon acceptance.

#### C. Comparison with the State-of-the-arts

We first compared our method with baseline models H-Sup and HL-Sup (V-Net architecture) and then with state-of-the-art methods, including label quality-agnostic (TriNet [13], 2SRnT [5], PNL [14], MS-TFAL [15]) and label quality-knowable approaches (Decoupled [17], MTCL-Hard, MTCL-FS, MTCL-UDS [11], MixSegNet [18]).

Fig. 4 visualizes results from the top four methods by Dice loss. ALC consistently generated masks closely aligned with the ground truth, underscoring its effectiveness. However, the failure cases highlighted by white circles in the last row reveal a sensitivity of  $\mathcal{L}_n$  to label quality. Future work will focus on improving data quality assessment and developing strategies to mitigate these sensitivities.

#### D. Ablation Studies

To evaluate the effectiveness of each component of the proposed method, we conducted extensive experiments on two datasets under different HQ labeled data settings (10%

TABLE I  
SEGMENTATION RESULTS ON THE NIH PANCREAS SEGMENTATION DATASET COMPARED WITH STATE-OF-THE-ART METHODS.

Methods	10% Set-HQ and 90% Set-LQ				20% Set-HQ and 80% Set-LQ			
	Dice [%]↑	Jaccard [%]↑	95HD [mm]↓	ASD [mm]↓	Dice [%]↑	Jaccard [%]↑	95HD [mm]↓	ASD [mm]↓
H-Sup	70.86	56.50	21.15	8.87	73.64	59.98	12.18	4.65
HL-Sup	69.45	54.68	22.18	9.75	72.90	58.68	13.72	4.83
TriNet [13]	73.76	59.59	21.48	6.77	76.13	62.23	9.35	3.84
2SRnT [5]	72.56	58.13	20.40	6.08	75.72	61.66	11.23	4.32
PNL [14]	72.67	57.93	19.42	6.19	76.95	63.22	9.57	3.83
MS-TFAL [15]	72.83	58.63	18.43	6.24	75.56	61.36	10.05	4.15
TBraTS [16]	71.19	56.92	23.06	7.06	75.28	61.21	8.69	4.95
Decoupled [17]	73.16	59.21	19.79	5.98	78.13	64.90	9.33	3.48
KDEM [10]	73.57	59.57	18.89	5.77	77.36	64.01	6.24	2.73
MTCL-Hard [11]	<u>74.88</u>	<u>60.49</u>	19.50	<u>5.54</u>	<u>78.97</u>	65.86	9.24	<u>2.13</u>
MTCL-FS [11]	73.95	60.01	18.33	6.17	77.65	64.17	9.83	3.07
MTCL-UDS [11]	74.30	59.94	19.54	6.09	78.19	<u>65.88</u>	7.21	2.32
MixSegNet [18]	74.06	59.66	<u>18.31</u>	6.46	77.07	63.94	8.22	2.76
ALC (ours)	<b>75.21</b>	<b>60.94</b>	<b>18.13</b>	<b>5.37</b>	<b>79.62</b>	<b>66.32</b>	<b>5.86</b>	<b>2.02</b>

TABLE II  
ABLATION STUDY ON LA DATASET.

10% Set-HQ and 90% Set-LQ				
Methods	Dice [%]↑	Jaccard [%]↑	95HD [mm]↓	ASD [mm]↓
Mean-Teacher [24]	83.79	72.62	20.07	4.01
ALC w/o LS	84.42	73.59	10.49	2.87
ALC w/o LR	<u>87.31</u>	<u>77.81</u>	<u>8.79</u>	<u>2.81</u>
ALC (ours)	<b>88.87</b>	<b>80.23</b>	<b>8.36</b>	<b>2.29</b>

20% Set-HQ and 80% Set-LQ				
Methods	Dice [%]↑	Jaccard [%]↑	95HD [mm]↓	ASD [mm]↓
Mean-Teacher [24]	87.51	77.92	8.83	2.86
ALC w/o LS	88.11	79.19	<u>6.76</u>	<u>1.99</u>
ALC w/o LR	<u>88.53</u>	<u>79.53</u>	9.13	2.77
ALC (ours)	<b>89.29</b>	<b>80.99</b>	<b>6.30</b>	<b>1.22</b>

TABLE III  
ABLATION STUDY ON NIH DATASET.

10% Set-HQ and 90% Set-LQ				
Methods	Dice [%]↑	Jaccard [%]↑	95HD [mm]↓	ASD [mm]↓
Mean-Teacher [24]	70.59	55.48	23.58	7.43
ALC w/o LS	71.17	56.12	22.56	6.38
ALC w/o LR	<u>73.23</u>	<u>58.66</u>	<u>19.67</u>	<u>6.51</u>
ALC (ours)	<b>75.21</b>	<b>60.94</b>	<b>18.13</b>	<b>5.37</b>

20% Set-HQ and 80% Set-LQ				
Methods	Dice [%]↑	Jaccard [%]↑	95HD [mm]↓	ASD [mm]↓
Mean-Teacher [24]	74.77	60.51	15.09	4.78
ALC w/o LS	75.48	61.50	11.07	3.96
ALC w/o LR	<u>76.23</u>	<u>62.29</u>	<u>10.45</u>	<u>3.74</u>
ALC (ours)	<b>79.62</b>	<b>66.32</b>	<b>5.86</b>	<b>2.02</b>

and 20%). Mean Teacher [24] was used as the baseline for ablation studies. The experiments included: 1) **ALC w/o LS**: the framework without label selection; and 2) **ALC w/o LR**: the framework without label refinement.

As shown in Tables II and III, each component significantly contributes to improved segmentation performance. Notably, removing label selection (ALC w/o LS) results in a more pronounced performance drop compared to removing label refinement (ALC w/o LR), indicating that selecting HQ labeled data has a greater impact than label refinement. However, the

combination of both components achieves the best results. Additionally, Table III reveals smaller performance gains compared to Table II, reflecting the varying difficulty levels across tasks. In all cases, as the proportion of HQ data increases, the performance improvement margin decreases.

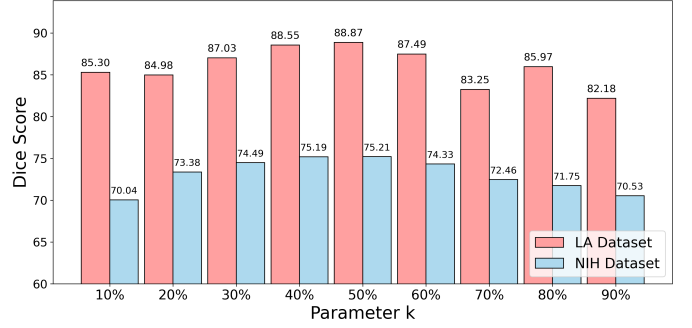


Fig. 5. The impact of different  $k$  values on the LA and NIH datasets under 10% HQ label data and 90% LQ label data.

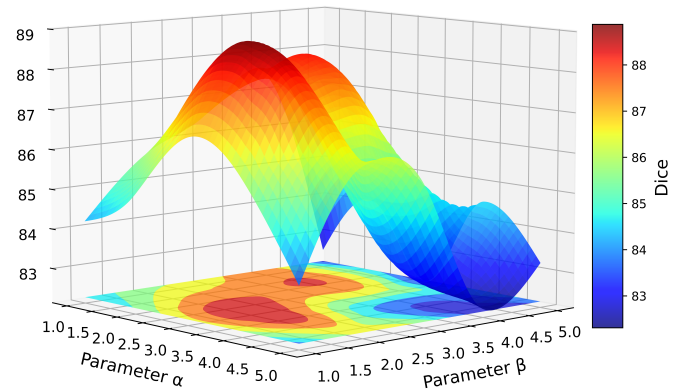


Fig. 6. Visualization of the impact of different  $\alpha$  and  $\beta$  values on NIH pancreas segmentation dataset under 10% HQ label data and 90% LQ label data. Where C denotes Dice score.

To further evaluate the label refinement method, we compared the quality of directly generated pseudo-labels with refined pseudo-labels for the top- $k$  samples, evaluated every



5,000 iterations. The results, visualized in Fig. 3, demonstrate that although there are occasional fluctuations where generated pseudo-labels outperform refined ones, label refinement consistently enhances overall performance. On the LA and NIH datasets, refined labels generally outperform directly generated pseudo-labels. This improvement is attributed to label refinement's ability to effectively capture perturbation-induced relationships, yielding more accurate pseudo-labels.

#### E. Parameter Sensitivity Analysis

To evaluate the impact of different values of  $k$ , experiments were conducted on the LA and NIH datasets, as shown in Fig. 5. The parameter  $k$  controls the proportion of low-quality labeled data in a mini-batch used for gradient updates. A smaller  $k$  reduces the inclusion of refined labels, offering limited benefits to the model, while a larger  $k$  increases the likelihood of incorporating lower-quality refined labels, potentially leading to performance degradation. Optimal performance is achieved at  $k = 0.5$ , which balances label quality and data utilization effectively.

Additionally, we analyzed the influence of  $\alpha$  and  $\beta$  on the NIH pancreas dataset, as shown in Fig. 6. These parameters modulate the contributions of  $\mathcal{L}_{ls}$  and  $\mathcal{L}_n$ , respectively. Larger values of  $\alpha$  and  $\beta$  can destabilize training by overemphasizing high-quality labels, while smaller values may hinder performance improvements. Optimal results are achieved at  $\alpha = 3$  and  $\beta = 2$ , ensuring effective supervision and stable training.

#### IV. CONCLUSION

This paper introduces an Adaptive Label Correction (ALC) framework designed for robust medical image segmentation. The framework employs a dynamic label refinement algorithm to adaptively weight multiple perturbation variants, improving the quality of noisy label data. Additionally, the overall confidence of each noisy labeled sample is evaluated, enabling the selective learning of high-confidence samples under low-quality label learning, while the remaining samples are processed through noisy label learning strategies. Comprehensive experiments on two public datasets demonstrate the effectiveness of each component in our proposed approach. Compared to the state-of-the-art methods, our framework demonstrates superior performance and robust competitiveness in managing noisy label data.

#### REFERENCES

- [1] R. Azad, E. K. Aghdam, A. Rauland, Y. Jia, A. H. Avval, A. Bozorgpour, S. Karimijafarbigloo, J. P. Cohen, E. Adeli, and D. Merhof, "Medical image segmentation review: The success of u-net," *IEEE Transactions on Pattern Analysis and Machine Intelligence*, 2024.
- [2] M. Heidari, A. Kazerouni, M. Soltany, R. Azad, E. K. Aghdam, J. Cohen-Adad, and D. Merhof, "Hiformer: Hierarchical multi-scale representations using transformers for medical image segmentation," in *WACV*, 2023, pp. 6202–6212.
- [3] K. Han, L. Liu, Y. Song, Y. Liu, C. Qiu, Y. Tang, Q. Teng, and Z. Liu, "An effective semi-supervised approach for liver ct image segmentation," *IEEE Journal of Biomedical and Health Informatics*, vol. 26, no. 8, pp. 3999–4007, 2022.
- [4] K. Han, V. S. Sheng, Y. Song, Y. Liu, C. Qiu, S. Ma, and Z. Liu, "Deep semi-supervised learning for medical image segmentation: A review," *Expert Systems with Applications*, p. 123052, 2024.
- [5] M. Zhang, J. Gao, Z. Lyu, W. Zhao, Q. Wang, W. Ding, S. Wang, Z. Li, and S. Cui, "Characterizing label errors: Confident learning for noisy-labeled image segmentation," in *MICCAI*. Springer, 2020, pp. 721–730.
- [6] C. Fang, Q. Wang, L. Cheng, Z. Gao, C. Pan, Z. Cao, Z. Zheng, and D. Zhang, "Reliable mutual distillation for medical image segmentation under imperfect annotations," *IEEE Transactions on Medical Imaging*, 2023.
- [7] S. Zhai, G. Wang, X. Luo, Q. Yue, K. Li, and S. Zhang, "Pa-seg: learning from point annotations for 3d medical image segmentation using contextual regularization and cross knowledge distillation," *IEEE Transactions on Medical Imaging*, 2023.
- [8] Z. Xu, D. Lu, Y. Wang, J. Luo, J. Jayender, K. Ma, Y. Zheng, and X. Li, "Noisy labels are treasure: mean-teacher-assisted confident learning for hepatic vessel segmentation," in *MICCAI*. Springer, 2021, pp. 3–13.
- [9] C. Qian, K. Han, J. Wang, Z. Yuan, R. Qian, C. Lyu, J. Chen, and Z. Liu, "Dyncim: Dynamic curriculum for imbalanced multimodal learning," *arXiv preprint arXiv:2503.06456*, 2025.
- [10] J. Dolz, C. Desrosiers, and I. B. Ayed, "Teach me to segment with mixed supervision: Confident students become masters," in *International Conference on Information Processing in Medical Imaging*. Springer, 2021, pp. 517–529.
- [11] Z. Xu, D. Lu, J. Luo, Y. Wang, J. Yan, K. Ma, Y. Zheng, and R. K.-Y. Tong, "Anti-interference from noisy labels: Mean-teacher-assisted confident learning for medical image segmentation," *IEEE Transactions on Medical Imaging*, vol. 41, no. 11, pp. 3062–3073, 2022.
- [12] A. Kendall and Y. Gal, "What uncertainties do we need in bayesian deep learning for computer vision?" *NeurIPS*, vol. 30, 2017.
- [13] T. Zhang, L. Yu, N. Hu, S. Lv, and S. Gu, "Robust medical image segmentation from non-expert annotations with tri-network," in *MICCAI*. Springer, 2020, pp. 249–258.
- [14] H. Zhu, J. Shi, and J. Wu, "Pick-and-learn: Automatic quality evaluation for noisy-labeled image segmentation," in *MICCAI*. Springer, 2019, pp. 576–584.
- [15] B. Cui, M. Zhang, M. Xu, A. Wang, W. Yuan, and H. Ren, "Rectifying noisy labels with sequential prior: Multi-scale temporal feature affinity learning for robust video segmentation," in *MICCAI*. Springer, 2023, pp. 90–100.
- [16] K. Zou, X. Yuan, X. Shen, M. Wang, and H. Fu, "Tbrats: Trusted brain tumor segmentation," in *MICCAI*. Springer, 2022, pp. 503–513.
- [17] W. Luo and M. Yang, "Semi-supervised semantic segmentation via strong-weak dual-branch network," in *ECCV*. Springer, 2020, pp. 784–800.
- [18] Z. Wang and C. Yang, "Mixsegnet: Fusing multiple mixed-supervisory signals with multiple views of networks for mixed-supervised medical image segmentation," *Engineering Applications of Artificial Intelligence*, vol. 133, p. 108059, 2024.
- [19] Z. Xiong, Q. Xia, Z. Hu, N. Huang, C. Bian, Y. Zheng, S. Vesal, N. Ravikumar, A. Maier, X. Yang *et al.*, "A global benchmark of algorithms for segmenting the left atrium from late gadolinium-enhanced cardiac magnetic resonance imaging," *Medical Image Analysis*, vol. 67, p. 101832, 2021.
- [20] S. Adiga, J. Dolz, and H. Lombaert, "Anatomically-aware uncertainty for semi-supervised image segmentation," *Medical Image Analysis*, vol. 91, p. 103011, 2024.
- [21] H. R. Roth, L. Lu, A. Farag, H.-C. Shin, J. Liu, E. B. Turkbey, and R. M. Summers, "Deeporgan: Multi-level deep convolutional networks for automated pancreas segmentation," in *MICCAI*. Springer, 2015, pp. 556–564.
- [22] S. Liu, Y. Li, Q.-w. Chai, and W. Zheng, "Region-scalable fitting-assisted medical image segmentation with noisy labels," *Expert Systems with Applications*, vol. 238, p. 121926, 2024.
- [23] F. Milletari, N. Navab, and S.-A. Ahmadi, "V-net: Fully convolutional neural networks for volumetric medical image segmentation," in *3DV*. IEEE, 2016, pp. 565–571.
- [24] A. Tarvainen and H. Valpola, "Mean teachers are better role models: Weight-averaged consistency targets improve semi-supervised deep learning results," *NeurIPS*, vol. 30, 2017.